

First measurement of the form factors in $D_s^+ \rightarrow K^0 e^+ \nu_e$ and $D_s^+ \rightarrow K^{*0} e^+ \nu_e$ decays

M. Ablikim¹, M. N. Achasov^{10,d}, S. Ahmed¹⁵, M. Albrecht⁴, M. Alekseev^{55A,55C}, A. Amoroso^{55A,55C}, F. F. An¹, Q. An^{52,42}, Y. Bai⁴¹, O. Bakina²⁷, R. Baldini Ferroli^{23A}, Y. Ban³⁵, K. Begzsuren²⁵, D. W. Bennett²², J. V. Bennett⁵, N. Berger²⁶, M. Bertani^{23A}, D. Bettoni^{24A}, F. Bianchi^{55A,55C}, E. Boger^{27,b}, I. Boyko²⁷, R. A. Briere⁵, H. Cai⁵⁷, X. Cai^{1,42}, A. Calcaterra^{23A}, G. F. Cao^{1,46}, S. A. Cetin^{45B}, J. Chai^{55C}, J. F. Chang^{1,42}, W. L. Chang^{1,46}, G. Chelkov^{27,b,c}, G. Chen¹, H. S. Chen^{1,46}, J. C. Chen¹, M. L. Chen^{1,42}, P. L. Chen⁵³, S. J. Chen³³, X. R. Chen³⁰, Y. B. Chen^{1,42}, W. Cheng^{55C}, X. K. Chu³⁵, G. Cibinetto^{24A}, F. Cossio^{55C}, H. L. Dai^{1,42}, J. P. Dai^{37,h}, A. Dbeysi¹⁵, D. Dedovich²⁷, Z. Y. Deng¹, A. Denig²⁶, I. Denysenko²⁷, M. Destefanis^{55A,55C}, F. De Mori^{55A,55C}, Y. Ding³¹, C. Dong³⁴, J. Dong^{1,42}, L. Y. Dong^{1,46}, M. Y. Dong^{1,42,46}, Z. L. Dou³³, S. X. Du⁶⁰, P. F. Duan¹, J. Fang^{1,42}, S. S. Fang^{1,46}, Y. Fang¹, R. Farinelli^{24A,24B}, L. Fava^{55B,55C}, S. Fegan²⁶, F. Feldbauer⁴, G. Felici^{23A}, C. Q. Feng^{52,42}, E. Fioravanti^{24A}, M. Fritsch⁴, C. D. Fu¹, Q. Gao¹, X. L. Gao^{52,42}, Y. Gao⁴⁴, Y. G. Gao⁶, Z. Gao^{52,42}, B. Garillon²⁶, I. Garzia^{24A}, A. Gilman⁴⁹, K. Goetzen¹¹, L. Gong³⁴, W. X. Gong^{1,42}, W. Gradl²⁶, M. Greco^{55A,55C}, L. M. Gu³³, M. H. Gu^{1,42}, Y. T. Gu¹³, A. Q. Guo¹, L. B. Guo³², R. P. Guo^{1,46}, Y. P. Guo²⁶, A. Guskov²⁷, Z. Haddadi²⁹, S. Han⁵⁷, X. Q. Hao¹⁶, F. A. Harris⁴⁷, K. L. He^{1,46}, X. Q. He⁵¹, F. H. Heinsius⁴, T. Held⁴, Y. K. Heng^{1,42,46}, Z. L. Hou¹, H. M. Hu^{1,46}, J. F. Hu^{37,h}, T. Hu^{1,42,46}, Y. Hu¹, G. S. Huang^{52,42}, J. S. Huang¹⁶, X. T. Huang³⁶, X. Z. Huang³³, Z. L. Huang³¹, T. Hussain⁵⁴, W. Ikegami Andersson⁵⁶, M. Irshad^{52,42}, Q. Ji¹, Q. P. Ji¹⁶, X. B. Ji^{1,46}, X. L. Ji^{1,42}, X. S. Jiang^{1,42,46}, X. Y. Jiang³⁴, J. B. Jiao³⁶, Z. Jiao¹⁸, D. P. Jin^{1,42,46}, S. Jin³³, Y. Jin⁴⁸, T. Johansson⁵⁶, A. Julin⁴⁹, N. Kalantar-Nayestanaki²⁹, X. S. Kang³⁴, M. Kavatsyuk²⁹, B. C. Ke¹, I. K. Keshk⁴, T. Khan^{52,42}, A. Khokuz⁵⁰, P. Kiese²⁶, R. Kiuchi¹, R. Kliemt¹¹, L. Koch²⁸, O. B. Kolcu^{45B,f}, B. Kopf⁴, M. Kornicer⁴⁷, M. Kuemmel⁴, M. Kuessner⁴, A. Kupsc⁵⁶, M. Kurth¹, W. Kühn²⁸, J. S. Lange²⁸, P. Larin¹⁵, L. Lavezzi^{55C}, S. Leiber⁴, H. Leithoff²⁶, C. Li⁵⁶, Cheng Li^{52,42}, D. M. Li⁶⁰, F. Li^{1,42}, F. Y. Li³⁵, G. Li¹, H. B. Li^{1,46}, H. J. Li^{1,46}, J. C. Li¹, J. W. Li⁴⁰, K. J. Li⁴³, Kang Li¹⁴, Ke Li¹, Lei Li³, P. L. Li^{52,42}, P. R. Li^{46,7}, Q. Y. Li³⁶, T. Li³⁶, W. D. Li^{1,46}, W. G. Li¹, X. L. Li³⁶, X. N. Li^{1,42}, X. Q. Li³⁴, Z. B. Li⁴³, H. Liang^{52,42}, Y. F. Liang³⁹, Y. T. Liang²⁸, G. R. Liao¹², L. Z. Liao^{1,46}, J. Libby²¹, C. X. Lin⁴³, D. X. Lin¹⁵, B. Liu^{37,h}, B. J. Liu¹, C. X. Liu¹, D. Liu^{52,42}, D. Y. Liu^{37,h}, F. H. Liu³⁸, Fang Liu¹, Feng Liu⁶, H. B. Liu¹³, H. L. Liu⁴¹, H. M. Liu^{1,46}, Huanhuan Liu¹, Huihui Liu¹⁷, J. B. Liu^{52,42}, J. Y. Liu^{1,46}, K. Y. Liu³¹, Ke Liu⁶, L. D. Liu³⁵, Q. Liu⁴⁶, S. B. Liu^{52,42}, X. Liu³⁰, Y. B. Liu³⁴, Z. A. Liu^{1,42,46}, Zhiqing Liu²⁶, Y. F. Long³⁵, X. C. Lou^{1,42,46}, H. J. Lu¹⁸, J. G. Lu^{1,42}, Y. Lu¹, Y. P. Lu^{1,42}, C. L. Luo³², M. X. Luo⁵⁹, T. Luo^{9,j}, X. L. Luo^{1,42}, S. Lusso^{55C}, X. R. Lyu⁴⁶, F. C. Ma³¹, H. L. Ma¹, L. L. Ma³⁶, M. M. Ma^{1,46}, Q. M. Ma¹, X. N. Ma³⁴, X. Y. Ma^{1,42}, Y. M. Ma³⁶, F. E. Maas¹⁵, M. Maggiora^{55A,55C}, S. Maldaner²⁶, Q. A. Malik⁵⁴, A. Mangoni^{23B}, Y. J. Mao³⁵, Z. P. Mao¹, S. Marcello^{55A,55C}, Z. X. Meng⁴⁸, J. G. Messchendorp²⁹, G. Mezzadri^{24A}, J. Min^{1,42}, T. J. Min³³, R. E. Mitchell²², X. H. Mo^{1,42,46}, Y. J. Mo⁶, C. Morales Morales¹⁵, N. Yu. Muchnoi^{10,d}, H. Muramatsu⁴⁹, A. Mustafa⁴, S. Nakhoul^{11,g}, Y. Nefedov²⁷, F. Nerling^{11,g}, I. B. Nikolaev^{10,d}, Z. Ning^{1,42}, S. Nisar⁸, S. L. Niu^{1,42}, X. Y. Niu^{1,46}, S. L. Olsen⁴⁶, Q. Ouyang^{1,42,46}, S. Pacetti^{23B}, Y. Pan^{52,42}, M. Papenbrock⁵⁶, P. Patteri^{23A}, M. Pelizaeus⁴, J. Pellegrino^{55A,55C}, H. P. Peng^{52,42}, Z. Y. Peng¹³, K. Peters^{11,g}, J. Pettersson⁵⁶, J. L. Ping³², R. G. Ping^{1,46}, A. Pitka⁴, R. Poling⁴⁹, V. Prasad^{52,42}, H. R. Qi², M. Qi³³, T. Y. Qi², S. Qian^{1,42}, C. F. Qiao⁴⁶, N. Qin⁵⁷, X. S. Qin⁴, Z. H. Qin^{1,42}, J. F. Qiu¹, S. Q. Qu³⁴, K. H. Rashid^{54,i}, C. F. Redmer²⁶, M. Richter⁴, M. Ripka²⁶, A. Rivetti^{55C}, M. Rolo^{55C}, G. Rong^{1,46}, Ch. Rosner¹⁵, A. Sarantsev^{27,e}, M. Savrié^{24B}, K. Schoenning⁵⁶, W. Shan¹⁹, X. Y. Shan^{52,42}, M. Shao^{52,42}, C. P. Shen², P. X. Shen³⁴, X. Y. Shen^{1,46}, H. Y. Sheng¹, X. Shi^{1,42}, J. J. Song³⁶, W. M. Song³⁶, X. Y. Song¹, S. Sosio^{55A,55C}, C. Sowa⁴, S. Spataro^{55A,55C}, G. X. Sun¹, J. F. Sun¹⁶, L. Sun⁵⁷, S. S. Sun^{1,46}, X. H. Sun¹, Y. J. Sun^{52,42}, Y. K. Sun^{52,42}, Y. Z. Sun¹, Z. J. Sun^{1,42}, Z. T. Sun¹, Y. T. Tan^{52,42}, C. J. Tang³⁹, G. Y. Tang¹, X. Tang¹, M. Tiemens²⁹, B. Tsednee²⁵, I. Uman^{45D}, B. Wang¹, B. L. Wang⁴⁶, C. W. Wang³³, D. Wang³⁵, D. Y. Wang³⁵, Dan Wang⁴⁶, K. Wang^{1,42}, L. L. Wang¹, L. S. Wang¹, M. Wang³⁶, Meng Wang^{1,46}, P. Wang¹, P. L. Wang¹, W. P. Wang^{52,42}, X. F. Wang¹, Y. Wang^{52,42}, Y. F. Wang^{1,42,46}, Z. Wang^{1,42}, Z. G. Wang^{1,42}, Z. Y. Wang¹, Zongyuan Wang^{1,46}, T. Weber⁴, D. H. Wei¹², P. Weidenkaff²⁶, S. P. Wen¹, U. Wiedner⁴, M. Wolke⁵⁶, L. H. Wu¹, L. J. Wu^{1,46}, Z. Wu^{1,42}, L. Xia^{52,42}, X. Xia³⁶, Y. Xia²⁰, D. Xiao¹, Y. J. Xiao^{1,46}, Z. J. Xiao³², Y. G. Xie^{1,42}, Y. H. Xie⁶, X. A. Xiong^{1,46}, Q. L. Xiu^{1,42}, G. F. Xu¹, J. J. Xu^{1,46}, L. Xu¹, Q. J. Xu¹⁴, X. P. Xu⁴⁰, F. Yan⁵³, L. Yan^{55A,55C}, W. B. Yan^{52,42}, W. C. Yan², Y. H. Yan²⁰, H. J. Yang^{37,h}, H. X. Yang¹, L. Yang⁵⁷, R. X. Yang^{52,42}, S. L. Yang^{1,46}, Y. H. Yang³³, Y. X. Yang¹², Yifan Yang^{1,46}, Z. Q. Yang²⁰, M. Ye^{1,42}, M. H. Ye⁷, J. H. Yin¹, Z. Y. You⁴³, B. X. Yu^{1,42,46}, C. X. Yu³⁴, J. S. Yu²⁰, J. S. Yu³⁰, C. Z. Yuan^{1,46}, Y. Yuan¹, A. Yuncu^{45B,a}, A. A. Zafar⁵⁴, Y. Zeng²⁰, B. X. Zhang¹, B. Y. Zhang^{1,42}, C. C. Zhang¹, D. H. Zhang¹, H. H. Zhang⁴³, H. Y. Zhang^{1,42}, J. Zhang^{1,46}, J. L. Zhang⁵⁸, J. Q. Zhang⁴, J. W. Zhang^{1,42,46}, J. Y. Zhang¹, J. Z. Zhang^{1,46}, K. Zhang^{1,46}, L. Zhang⁴⁴, S. F. Zhang³³, T. J. Zhang^{37,h}, X. Y. Zhang³⁶, Y. Zhang^{52,42}, Y. H. Zhang^{1,42}, Y. T. Zhang^{52,42}, Yang Zhang¹, Yao Zhang¹, Yu Zhang⁴⁶, Z. H. Zhang⁶, Z. P. Zhang⁵², Z. Y. Zhang⁵⁷, G. Zhao¹, J. W. Zhao^{1,42}, J. Y. Zhao^{1,46}, J. Z. Zhao^{1,42}, Lei Zhao^{52,42}, Ling Zhao¹, M. G. Zhao³⁴, Q. Zhao¹, S. J. Zhao⁶⁰, T. C. Zhao¹, Y. B. Zhao^{1,42}, Z. G. Zhao^{52,42}, A. Zhemchugov^{27,b}, B. Zheng⁵³, J. P. Zheng^{1,42}, W. J. Zheng³⁶, Y. H. Zheng⁴⁶, B. Zhong³², L. Zhou^{1,42}, Q. Zhou^{1,46}, X. Zhou⁵⁷, X. K. Zhou^{52,42}, X. R. Zhou^{52,42}, X. Y. Zhou¹, Xiaoyu Zhou²⁰, Xu Zhou²⁰, A. N. Zhu^{1,46}, J. Zhu³⁴, J. Zhu⁴³, K. Zhu¹, K. J. Zhu^{1,42,46}, S. Zhu¹, S. H. Zhu⁵¹, X. L. Zhu⁴⁴, Y. C. Zhu^{52,42}, Y. S. Zhu^{1,46}, Z. A. Zhu^{1,46}, J. Zhuang^{1,42}, B. S. Zou¹, J. H. Zou¹

(BESIII Collaboration)

¹ Institute of High Energy Physics, Beijing 100049, People's Republic of China² Beihang University, Beijing 100191, People's Republic of China³ Beijing Institute of Petrochemical Technology, Beijing 102617, People's Republic of China⁴ Bochum Ruhr-University, D-44780 Bochum, Germany⁵ Carnegie Mellon University, Pittsburgh, Pennsylvania 15213, USA⁶ Central China Normal University, Wuhan 430079, People's Republic of China⁷ China Center of Advanced Science and Technology, Beijing 100190, People's Republic of China⁸ COMSATS Institute of Information Technology, Lahore, Defence Road, Off Raiwind Road, 54000 Lahore, Pakistan⁹ Fudan University, Shanghai 200443, People's Republic of China¹⁰ G.I. Budker Institute of Nuclear Physics SB RAS (BINP), Novosibirsk 630090, Russia¹¹ GSI Helmholtzcentre for Heavy Ion Research GmbH, D-64291 Darmstadt, Germany

- ¹² Guangxi Normal University, Guilin 541004, People's Republic of China
¹³ Guangxi University, Nanning 530004, People's Republic of China
¹⁴ Hangzhou Normal University, Hangzhou 310036, People's Republic of China
¹⁵ Helmholtz Institute Mainz, Johann-Joachim-Becher-Weg 45, D-55099 Mainz, Germany
¹⁶ Henan Normal University, Xinxiang 453007, People's Republic of China
¹⁷ Henan University of Science and Technology, Luoyang 471003, People's Republic of China
¹⁸ Huangshan College, Huangshan 245000, People's Republic of China
¹⁹ Hunan Normal University, Changsha 410081, People's Republic of China
²⁰ Hunan University, Changsha 410082, People's Republic of China
²¹ Indian Institute of Technology Madras, Chennai 600036, India
²² Indiana University, Bloomington, Indiana 47405, USA
²³ (A)INFN Laboratori Nazionali di Frascati, I-00044, Frascati, Italy; (B)INFN and University of Perugia, I-06100, Perugia, Italy
²⁴ (A)INFN Sezione di Ferrara, I-44122, Ferrara, Italy; (B)University of Ferrara, I-44122, Ferrara, Italy
²⁵ Institute of Physics and Technology, Peace Ave. 54B, Ulaanbaatar 13330, Mongolia
²⁶ Johannes Gutenberg University of Mainz, Johann-Joachim-Becher-Weg 45, D-55099 Mainz, Germany
²⁷ Joint Institute for Nuclear Research, 141980 Dubna, Moscow region, Russia
²⁸ Justus-Liebig-Universitaet Giessen, II. Physikalisches Institut, Heinrich-Buff-Ring 16, D-35392 Giessen, Germany
²⁹ KVI-CART, University of Groningen, NL-9747 AA Groningen, The Netherlands
³⁰ Lanzhou University, Lanzhou 730000, People's Republic of China
³¹ Liaoning University, Shenyang 110036, People's Republic of China
³² Nanjing Normal University, Nanjing 210023, People's Republic of China
³³ Nanjing University, Nanjing 210093, People's Republic of China
³⁴ Nankai University, Tianjin 300071, People's Republic of China
³⁵ Peking University, Beijing 100871, People's Republic of China
³⁶ Shandong University, Jinan 250100, People's Republic of China
³⁷ Shanghai Jiao Tong University, Shanghai 200240, People's Republic of China
³⁸ Shanxi University, Taiyuan 030006, People's Republic of China
³⁹ Sichuan University, Chengdu 610064, People's Republic of China
⁴⁰ Soochow University, Suzhou 215006, People's Republic of China
⁴¹ Southeast University, Nanjing 211100, People's Republic of China
⁴² State Key Laboratory of Particle Detection and Electronics, Beijing 100049, Hefei 230026, People's Republic of China
⁴³ Sun Yat-Sen University, Guangzhou 510275, People's Republic of China
⁴⁴ Tsinghua University, Beijing 100084, People's Republic of China
⁴⁵ (A)Ankara University, 06100 Tandogan, Ankara, Turkey; (B)Istanbul Bilgi University, 34060 Eyup, Istanbul, Turkey; (C)Uludag University, 16059 Bursa, Turkey; (D)Near East University, Nicosia, North Cyprus, Mersin 10, Turkey
⁴⁶ University of Chinese Academy of Sciences, Beijing 100049, People's Republic of China
⁴⁷ University of Hawaii, Honolulu, Hawaii 96822, USA
⁴⁸ University of Jinan, Jinan 250022, People's Republic of China
⁴⁹ University of Minnesota, Minneapolis, Minnesota 55455, USA
⁵⁰ University of Muenster, Wilhelm-Klemm-Str. 9, 48149 Muenster, Germany
⁵¹ University of Science and Technology Liaoning, Anshan 114051, People's Republic of China
⁵² University of Science and Technology of China, Hefei 230026, People's Republic of China
⁵³ University of South China, Hengyang 421001, People's Republic of China
⁵⁴ University of the Punjab, Lahore-54590, Pakistan
⁵⁵ (A)University of Turin, I-10125, Turin, Italy; (B)University of Eastern Piedmont, I-15121, Alessandria, Italy; (C)INFN, I-10125, Turin, Italy
⁵⁶ Uppsala University, Box 516, SE-75120 Uppsala, Sweden
⁵⁷ Wuhan University, Wuhan 430072, People's Republic of China
⁵⁸ Xinyang Normal University, Xinyang 464000, People's Republic of China
⁵⁹ Zhejiang University, Hangzhou 310027, People's Republic of China
⁶⁰ Zhengzhou University, Zhengzhou 450001, People's Republic of China

^a Also at Bogazici University, 34342 Istanbul, Turkey

^b Also at the Moscow Institute of Physics and Technology, Moscow 141700, Russia

^c Also at the Functional Electronics Laboratory, Tomsk State University, Tomsk, 634050, Russia

^d Also at the Novosibirsk State University, Novosibirsk, 630090, Russia

^e Also at the NRC "Kurchatov Institute", PNPI, 188300, Gatchina, Russia

^f Also at Istanbul Arel University, 34295 Istanbul, Turkey

^g Also at Goethe University Frankfurt, 60323 Frankfurt am Main, Germany

^h Also at Key Laboratory for Particle Physics, Astrophysics and Cosmology, Ministry of Education; Shanghai Key Laboratory for Particle Physics and Cosmology; Institute of Nuclear and Particle Physics, Shanghai 200240, People's Republic of China

ⁱ Also at Government College Women University, Sialkot - 51310, Punjab, Pakistan.

^j Also at Key Laboratory of Nuclear Physics and Ion-beam Application (MOE) and Institute of Modern Physics, Fudan University, Shanghai 200443, People's Republic of China

We report on new measurements of Cabibbo-suppressed semileptonic D_s^+ decays using 3.19 fb^{-1} of e^+e^- annihilation data sample collected at a center-of-mass energy of 4.178 GeV with the BESIII detector at the BEPCII collider. Our results include branching fractions $\mathcal{B}(D_s^+ \rightarrow K^0 e^+ \nu_e) = (3.25 \pm 0.38(\text{stat.}) \pm 0.16(\text{syst.})) \times 10^{-3}$ and $\mathcal{B}(D_s^+ \rightarrow K^{*0} e^+ \nu_e) = (2.37 \pm 0.26(\text{stat.}) \pm 0.20(\text{syst.})) \times 10^{-3}$ which are much improved relative to previous measurements, and the first measurements of the hadronic form-factor parameters for these decays. For $D_s^+ \rightarrow K^0 e^+ \nu_e$, we obtain $f_+(0) = 0.720 \pm 0.084(\text{stat.}) \pm 0.013(\text{syst.})$, and for $D_s^+ \rightarrow K^{*0} e^+ \nu_e$, we find form-factor ratios $r_V = V(0)/A_1(0) = 1.67 \pm 0.34(\text{stat.}) \pm 0.16(\text{syst.})$ and $r_2 = A_2(0)/A_1(0) = 0.77 \pm 0.28(\text{stat.}) \pm 0.07(\text{syst.})$.

PACS numbers: 13.30.Ce, 14.40.Lb, 14.65.Dw

The study of D_s^+ semileptonic (SL) decays provides valuable information about weak and strong interactions in mesons composed of heavy quarks. (Throughout this Letter, charge-conjugate modes are implied unless explicitly noted.) Measurement of the total SL decay width of the D_s^+ , and comparison with that of the D mesons, can help elucidate the role of nonperturbative effects in heavy-meson decays [1, 2]. The Cabibbo-suppressed (CS) SL decays, including the branching fractions (BFs) for $D_s^+ \rightarrow K^0 e^+ \nu_e$ and $D_s^+ \rightarrow K^{*0} e^+ \nu_e$ [3], are especially poorly measured. Detailed investigations of the dynamics of these decays allow measurements of SL decay partial widths, which depend on the hadronic form factors (FFs) describing the interaction between the final-state quarks. Measurements of these FFs provide experimental tests of theoretical predictions of Lattice QCD (LQCD). Reference [4] predicts that the FFs have minimal dependence on the spectator-quark mass, with values for $D_s^+ \rightarrow K^0 \ell^+ \nu_\ell$ and $D^+ \rightarrow \pi^0 \ell^+ \nu_\ell$ differing by less than 5%. Experimental verification of this predicted instance of U -spin ($d \leftrightarrow s$) symmetry would be a significant success for LQCD. A complementary LQCD test is provided by comparing measured and predicted FF parameters for $D_s^+ \rightarrow K^{*0} \ell^+ \nu_\ell$ and $D^+ \rightarrow \rho^0 \ell^+ \nu_\ell$. The combination of these measurements has the potential to verify LQCD FF predictions for SL charm decays to both pseudoscalar and vector mesons, useful for further applying the LQCD to SL B decays for precise determination of Cabibbo-Kobayashi-Maskawa (CKM) parameters [4, 5].

In this Letter, we report on improved measurements of the absolute BFs and first measurements of the FFs for the decays $D_s^+ \rightarrow K^0 e^+ \nu_e$ and $D_s^+ \rightarrow K^{*0} e^+ \nu_e$. Our measurements have been made with 3.19 fb^{-1} e^+e^- annihilation data recorded with the BESIII detector at the BEPCII collider. The center-of-mass energy for our data is $\sqrt{s} = 4.178 \text{ GeV}$. The cross section is $\sim 1 \text{ nb}$ for the production of $D_s^{*+} D_s^- + c.c.$ at this energy. Our data sample is the largest collected by any experiment for D_s^+ studies in the clean near-threshold environment.

Details about the BESIII detector design and performance are provided in Ref. [6]. A GEANT4-based [7] Monte Carlo (MC) simulation package, which includes the geometric description of the detector and the detector response, is used to determine signal detection efficiencies and to estimate potential backgrounds. Signal MC samples of $e^+e^- \rightarrow D_s^{*+} D_s^-$ with a D_s^+ meson decaying to $K^{(*)0} e^+ \nu_e$ together with a

D_s^- decaying to the studied decay modes used for this analysis are generated with CONEXC [8] using EVTGEN [10], with initial-state radiation (ISR) [8, 9] and final-state radiation (FSR) effects [11] included. The simulation of the SL decay $D_s^+ \rightarrow K^{*0} e^+ \nu_e$ is matched with the FFs measured in this work. To study the backgrounds, inclusive MC samples consisting of open-charm states, radiative return to J/ψ and $\psi(2S)$ and continuum processes are generated. All known decay modes of open-charm and ψ states are simulated as specified by the Particle Data Group (PDG) [12], while the remaining unknown decays are modeled with LUNDCHARM [13].

As described above, D_s^+ mesons are produced at $\sqrt{s} = 4.178 \text{ GeV}$ predominantly through $D_s^{*+} D_s^-$ [14], with 94% of the D_s^{*+} decaying to γD_s^+ . The first step of our analysis is to select ‘‘single-tag’’ (ST) events with a fully reconstructed D_s^- candidate. The D_s^- hadronic decay tag modes that are used for this analysis are listed in Table I. In this ST sample, we select the SL decay $D_s^+ \rightarrow K^{(*)0} e^+ \nu_e$ plus an isolated photon consistent with being from the $D_s^* \rightarrow \gamma D_s$ transition. The selected events are referred to as the double-tag (DT) sample. For a specific tag mode i , the ST and DT event yields can be expressed as

$$N_{\text{ST}}^i = 2N_{D_s D_s^*} \mathcal{B}_{\text{ST}}^i \epsilon_{\text{ST}}^i \quad \text{and} \quad N_{\text{DT}}^i = 2N_{D_s D_s^*} \mathcal{B}_{\text{ST}}^i \mathcal{B}_{\text{SL}}^i \epsilon_{\text{DT}}^i,$$

where $N_{D_s D_s^*}$ is the number of $D_s D_s^*$ pairs; $\mathcal{B}_{\text{ST}}^i$ and $\mathcal{B}_{\text{SL}}^i$ are the BFs of the D_s^- tag mode and the D_s^+ SL decay mode, respectively; ϵ_{ST}^i is the efficiency for finding the tag candidate; and ϵ_{DT}^i is the efficiency for simultaneously finding the tag D_s^- and the SL decay. The DT efficiency ϵ_{DT}^i includes the BF for $D_s^{*+} \rightarrow \gamma D_s^+$. The BF for the SL decay is given by

$$\mathcal{B}_{\text{SL}} = \frac{N_{\text{DT}}}{\sum N_{\text{ST}}^i \times \epsilon_{\text{DT}}^i / \epsilon_{\text{ST}}^i} = \frac{N_{\text{DT}}}{N_{\text{ST}} \times \epsilon_{\text{SL}}}, \quad (1)$$

where N_{DT} is the total yield of DT events, N_{ST} is the total ST yield, and $\epsilon_{\text{SL}} = \frac{\sum N_{\text{ST}}^i \times \epsilon_{\text{DT}}^i / \epsilon_{\text{ST}}^i}{\sum N_{\text{ST}}^i}$ is the average efficiency for finding SL decay weighted by the measured yields of tag modes in data.

Selection criteria for photons, charged pions and charged kaons are the same as those used in Ref. [15]. To reconstruct π^0 and η candidates, the invariant masses of the accepted photon pairs must be within $(0.115, 0.150) \text{ GeV}/c^2$ and $(0.50, 0.57) \text{ GeV}/c^2$, respectively. To improve the momentum resolution, a kinematic fit is performed to constrain the $\gamma\gamma$ invariant mass to the nominal π^0 or η mass [3], and

TABLE I. $M_{D_s^-}$ windows and ST yields in data.

ST mode	$M_{D_s^-}$ (GeV/ c^2)	N_{ST}^i
$K_S^0 K^-$	(1.945, 1.990)	25858 ± 217
$K^+ K^- \pi^-$	(1.945, 1.990)	130666 ± 575
$K_S^0 K^- \pi^0$	(1.940, 1.990)	10807 ± 398
$K_S^0 K_S^0 \pi^-$	(1.945, 1.990)	3810 ± 131
$K^+ K^- \pi^- \pi^0$	(1.940, 1.990)	35091 ± 702
$K_S^0 K^- \pi^+ \pi^-$	(1.945, 1.990)	7722 ± 235
$K_S^0 K^+ \pi^- \pi^-$	(1.945, 1.990)	14802 ± 259
$\pi^+ \pi^- \pi^-$	(1.945, 1.990)	36258 ± 832
$\pi^- \eta$	(1.940, 1.990)	17535 ± 400
$\rho^- \eta$	(1.940, 1.990)	30114 ± 886
$\pi^- \eta' (\eta' \rightarrow \pi^+ \pi^- \eta)$	(1.940, 1.990)	7704 ± 152
$\rho^- \eta' (\eta' \rightarrow \pi^+ \pi^- \eta)$	(1.940, 1.990)	3039 ± 226
$\pi^- \eta' (\eta' \rightarrow \gamma \pi^+ \pi^-)$	(1.940, 1.990)	17919 ± 481

the χ^2 of the kinematic fit is required to be less than 20. The fitted π^0 and η momenta are used for reconstruction of the D_s^- tag candidates. K_S^0 mesons are reconstructed from two oppositely charged tracks with its invariant mass within (0.485, 0.510) GeV/ c^2 . A fit is applied to constrain these two charged tracks to a common vertex, and this K_S^0 decay vertex is required to be separated from the interaction point by more than twice the standard deviation of the measured flight distance. We select $\rho^- \rightarrow \pi^- \pi^0$ by requiring the invariant mass $M_{\pi^- \pi^0}$ to be within (0.626, 0.924) GeV/ c^2 [3]. The decay modes $\eta' \rightarrow \pi^+ \pi^- \eta$ and $\eta' \rightarrow \gamma \pi^+ \pi^-$ are used to select η' mesons, with the invariant masses of the $\pi^+ \pi^- \eta$ and $\gamma \pi^+ \pi^-$ required to be within (0.940, 0.976) GeV/ c^2 and (0.940, 0.970) GeV/ c^2 , respectively. Additionally, to suppress backgrounds from D^* decays, the momenta of the photons from $\eta' \rightarrow \gamma \pi^+ \pi^-$ and all pions are required to be greater than 0.1 GeV/ c .

For all events passing the ST selection criteria, we calculate the recoil mass against the tag with the following formula:

$$M_{\text{rec}} = \sqrt{(\sqrt{s} - \sqrt{|\vec{p}_{D_s^-}|^2 + m_{D_s^-}^2})^2 - |\vec{p}_{D_s^-}|^2},$$

where $m_{D_s^-}$ and $\vec{p}_{D_s^-}$ are the known mass [3] and measured momentum of the tag D_s^- . We define $\Delta M \equiv M_{\text{rec}} - m_{D_s^{*+}}$, where $m_{D_s^{*+}}$ is the nominal D_s^{*+} mass [3]. Events within $-0.060 < \Delta M < 0.065$ GeV/ c^2 are accepted as $D_s^{*+} D_s^-$ candidates. To extract the mode-by-mode ST yields, we perform unbinned maximum likelihood fits to the distributions of the D_s^- invariant mass $M_{D_s^-}$, as shown in Fig. 1. Signals are modeled with the MC-simulated signal shape convoluted with Gaussians to account for the resolution differences between data and MC, while the combinatorial backgrounds are parameterized with second- or third-order polynomial functions. Due to misidentification of π^- as K^- , the backgrounds from $D^- \rightarrow K_S^0 \pi^-$ form a broad peak near the D_s^- nominal mass for $D_s^- \rightarrow K_S^0 K^-$. In the fit, the shape of this background is described by using the MC simulation and its size is set as a

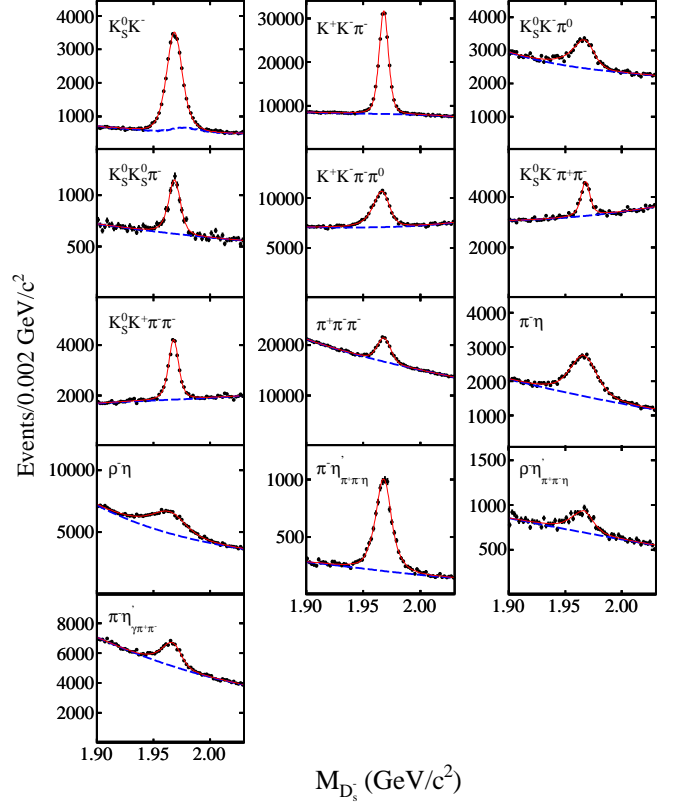


FIG. 1. (Color online) Fits to $M_{D_s^-}$ distributions for the thirteen tag modes. Points with error bars are data, blue dashed curves are the fitted backgrounds and red solid curves are the total fits.

free parameter. For each tag mode, the ST yield is obtained by integrating the signal function over the D_s^- mass signal region specified in the second column of Table I, which also includes the ST yields for all tag modes. The total reconstructed ST yield in our data sample is $N_{ST} = 341, 325 \pm 1, 764$.

In signal events, the system recoiling against the D_s^- tag consists of the SL decay $D_s^+ \rightarrow K^0 e^+ \nu_e$ or $D_s^+ \rightarrow K^{*0} e^+ \nu_e$. We select these from the additional tracks accompanying the tag, that is a $K^0 \rightarrow K_S^0 \rightarrow \pi^+ \pi^-$ with the ST criteria already described, and $K^{*0} \rightarrow K^+ \pi^-$ therefore requiring that there be exactly three tracks in the event and with the invariant mass $M_{K^+ \pi^-}$ required to be within (0.801, 0.991) GeV/ c^2 . For electron particle identification (PID), measurements of the specific ionization energy loss (dE/dx), the time of flight (TOF) and shower properties from the electromagnetic calorimeter (EMC) are used to construct probabilities for electron, pion and kaon hypotheses (\mathcal{L}_e , \mathcal{L}_π and \mathcal{L}_K). Electron candidates must satisfy $\mathcal{L}_e > 0.001$ and $\mathcal{L}_e / (\mathcal{L}_e + \mathcal{L}_\pi + \mathcal{L}_K) > 0.8$. Energy loss due to bremsstrahlung is partially recovered by adding the energy of EMC showers that are within 5° of the electron direction and not matched to other particles [16, 17]. Backgrounds from $D_s^+ \rightarrow K^0 \pi^+$ reconstructed as $D_s^+ \rightarrow K^0 e^+ \nu_e$ and $D_s^+ \rightarrow K^+ \pi^+ \pi^-$ re-

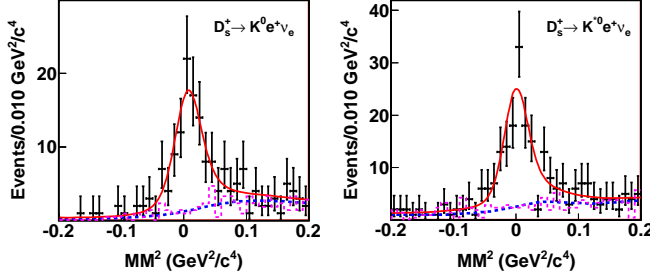


FIG. 2. (Color online) Fits to MM^2 distributions of SL candidate events. Dots with error bars are data, dot-dashed lines (blue) are the fitted backgrounds and solid curves (red) are the total fits. The long-dashed lines (pink) show the backgrounds from the $M_{D_s^-}$ sidebands.

constructed as $D_s^+ \rightarrow K^{*0} e^+ \nu_e$ are rejected by requiring the $K^0 e^+$ or $K^{*0} e^+$ invariant mass to be less than $1.78 \text{ GeV}/c^2$. Backgrounds associated with fake photons are suppressed by requiring $E_{\gamma_{\text{max}}}$, the largest energy of any unused photon, to be less than 0.20 GeV .

To identify a photon produced directly from $D_s^{*\pm}$, we perform two kinematic fits for each γ candidate, one assuming that the γ combines with the tag to form a D_s^{*-} and the other assuming that the SL decay comes from a D_s^{*+} parent. We require the $D_s^+ D_s^{*\pm}$ pair to conserve energy and momentum in the center-of-mass frame, and the D_s^\pm candidates are constrained to the known mass. The neutrino is treated as a missing particle. When we assume the tag to be the daughter of a D_s^{*-} , we constrain the mass of the photon plus tag candidate to be consistent with the expected D_s^{*-} mass; otherwise we constrain the mass of the photon plus SL decay to be consistent with the D_s^{*+} mass. Finally, we select the photon and hypothesis with the smallest kinematic fit χ^2 .

We obtain information about the undetected neutrino with the missing-mass squared of the event, calculated from the energies and momenta of the tag ($E_{D_s^-}$, $\vec{p}_{D_s^-}$), the transition photon (E_γ , \vec{p}_γ), and the detected SL decay products ($E_{\text{SL}} = E_{K^{(*)0}} + E_{e^+}$, $\vec{p}_{\text{SL}} = \vec{p}_{K^{(*)0}} + \vec{p}_{e^+}$) as follows:

$$MM^2 = (\sqrt{s} - E_{D_s^-} - E_\gamma - E_{\text{SL}})^2 - (|\vec{p}_{D_s^-} + \vec{p}_\gamma + \vec{p}_{\text{SL}}|)^2.$$

Figure 2 shows the MM^2 distributions of the accepted candidate events for $D_s^+ \rightarrow K^0 e^+ \nu_e$ and $D_s^+ \rightarrow K^{*0} e^+ \nu_e$ in data. The signal DT yield N_{DT} is obtained by performing an unbinned maximum likelihood fit to MM^2 . In the fit, the signal is described with an MC-derived signal shape convolved with a Gaussian, and the background is described by a shape obtained from the inclusive MC sample, in which no peaking backgrounds are observed. We obtain 117.2 ± 13.9 and 155.0 ± 17.2 events for $D_s^+ \rightarrow K^0 e^+ \nu_e$ and $D_s^+ \rightarrow K^{*0} e^+ \nu_e$, respectively, where the uncertainties are statistical only. No peaking backgrounds are observed in $K^{(*)0}$ mass sideband.

The BFs of $D_s^+ \rightarrow K^0 e^+ \nu_e$ and $D_s^+ \rightarrow K^{*0} e^+ \nu_e$ are determined by Eq. (1), where the detection efficiencies ε_{SL} are estimated to be $(10.57 \pm 0.04)\%$ and $(19.15 \pm 0.06)\%$

for $D_s^+ \rightarrow K^0 e^+ \nu_e$ and $D_s^+ \rightarrow K^{*0} e^+ \nu_e$, respectively. (These efficiencies include the BFs for $K^0 \rightarrow \pi^+ \pi^-$ and $K^{*0} \rightarrow K^+ \pi^-$.) Finally, we obtain $\mathcal{B}(D_s^+ \rightarrow K^0 e^+ \nu_e) = (3.25 \pm 0.38) \times 10^{-3}$ and $\mathcal{B}(D_s^+ \rightarrow K^{*0} e^+ \nu_e) = (2.37 \pm 0.26) \times 10^{-3}$, where the uncertainties are statistical only.

With the DT technique, the BF measurements are insensitive to the systematic uncertainties of the ST selection. The uncertainties of the e^+ tracking and PID efficiencies have all been determined to be 1.0% [17], while the uncertainty of the $K^{(*)0}$ reconstruction is 1.5 (2.3)%. The uncertainty associated with the MM^2 fit is estimated to be 3.5 (3.8)% by varying the fitting ranges and the signal and background shapes. The uncertainty due to the selection of the γ is estimated to be 2.0% based on selecting the best photon candidate in a control sample of $e^+ e^- \rightarrow D_s^{*+} D_s^-$ events with two hadronic tags, $D_s^+ \rightarrow K_S^0 K^+$ and $D_s^- \rightarrow K^+ K^- \pi^-$. The uncertainties due to the $E_{\gamma_{\text{max}}}$ and $M_{K^{(*)0} e^+}$ requirements are estimated to be 1.7 (1.7)% and 0.7 (0.9)% by comparing the nominal BF with that measured with alternative requirements. The uncertainty due to the MC signal modeling is estimated to be 0.9 (1.8)% by varying the input FF parameters by $\pm 1\sigma$ as determined in this work. We also consider the systematic uncertainties of N_{ST} (0.5%), evaluated by using alternative signal shapes when fitting the $M_{D_s^-}$ spectra, and of the MC statistics (0.4 [0.3]%). The uncertainty due to different tag dependencies between data and MC simulation is estimated to be 0.8 (0.3)%. Additionally, for $D_s^+ \rightarrow K^{*0} e^+ \nu_e$ decay, the systematic uncertainty for the possible \mathcal{S} -wave component in $K\pi$ system is estimated to be 6.0% according to Refs. [18, 19]. Adding these contributions in quadrature gives total systematic uncertainties of 5.1% and 8.3% for $\mathcal{B}(D_s^+ \rightarrow K^0 e^+ \nu_e)$ and $\mathcal{B}(D_s^+ \rightarrow K^{*0} e^+ \nu_e)$, respectively.

The $D_s^+ \rightarrow K^0 e^+ \nu_e$ differential decay width with respect to the mass squared (q^2) of the $e^+ \nu_e$ system is expressed as [20]:

$$\frac{d\Gamma(D_s^+ \rightarrow K^0 e^+ \nu_e)}{dq^2} = \frac{G_F^2 |V_{cd}|^2}{24\pi^3} p_{K^0}^3 |f_+^K(q^2)|^2. \quad (2)$$

In this equation p_{K^0} is the K^0 momentum in the rest frame of the D_s^+ , G_F is the Fermi constant [3], $|V_{cd}|$ is the CKM matrix element, and $f_+^K(q^2)$ is the hadronic FF. To extract the FF parameters, we fit to the differential decay rates $\Delta\Gamma_i$ measured in the q^2 bins of $[0.00, 0.35)$, $[0.35, 0.70)$, $[0.70, 1.05)$, $[1.05, 1.40)$ and $[1.40, 2.16) \text{ GeV}^2/c^2$ by using the three theoretical parameterizations in Table II. A least- χ^2 fit is performed accounting for correlations among q^2 bins. We fix the pole mass m_{pole} at the D^{*+} nominal mass [3]. The fits to the differential decay rate and projections of the fits onto $f_+(q^2)$ for $D_s^+ \rightarrow K^0 e^+ \nu_e$ are shown in Figs. 3(a) and (b), and the FF fit results are summarized in the third column of Table II. The systematic uncertainties in the extracted parameters are estimated as in Ref. [21]. These include the same systematic effects as the BF measurements, along with the D_s^+ -lifetime uncertainty. Using $|V_{cd}| = 0.22492 \pm 0.00050$ [3], we obtain $f_+^K(0)$ as shown in the last column of Table II.

TABLE II. FF results from fits to $D_s^+ \rightarrow K^0 e^+ \nu_e$, where the first errors are statistical and the second systematic.

Parameterizations	$f_+^K(0) V_{cd} $	$f_+^K(0)$
Simple pole [22]	$0.172 \pm 0.010 \pm 0.001$	$0.765 \pm 0.044 \pm 0.004$
Modified pole [22]	$0.163 \pm 0.017 \pm 0.003$	$0.725 \pm 0.076 \pm 0.013$
z series (2 par.) [23]	$0.162 \pm 0.019 \pm 0.003$	$0.720 \pm 0.084 \pm 0.013$

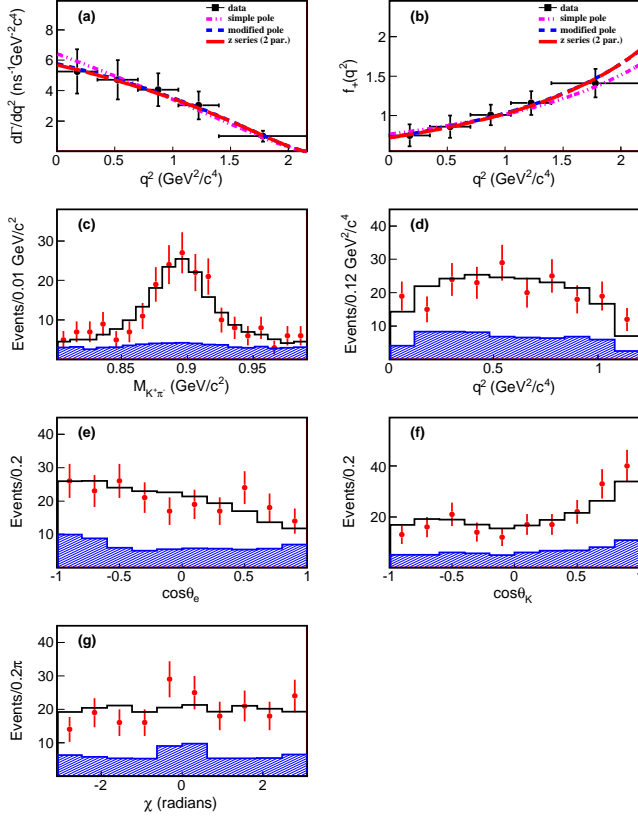


FIG. 3. (Color online) (a) Fits to the differential decay rates and (b) projections onto $f_+^K(q^2)$ for $D_s^+ \rightarrow K^0 e^+ \nu_e$. Projections onto (c) $M_{K^+\pi^-}$, (d) q^2 , (e) $\cos\theta_e$, (f) $\cos\theta_K$, and (g) χ for $D_s^+ \rightarrow K^0 e^+ \nu_e$. Dots with error bars are data. Curves in (a, b) give the best fits with different FF parameterizations. Solid and shadowed histograms in (c, d, e, f, g) are the MC-simulated signal plus background and the MC-simulated background.

The differential decay rate of $D_s^+ \rightarrow K^0 e^+ \nu_e$ depends on five variables: $K\pi$ mass-squared ($m_{K\pi}^2$), $e^+ \nu_e$ mass-squared (q^2), the angle between the K^+ and D_s^+ momenta in the $K\pi$ rest frame (θ_K), the angle between the ν_e and D_s^+ momenta in the $e^+ \nu_e$ system (θ_e), and the acoplanarity angle between the $K\pi$ and $e^+ \nu_e$ decay planes (χ). The differential decay rate can be expressed in terms of three helicity amplitudes [24, 25]: $H_\pm(q^2) = (M_{D_s^+} + m_{K\pi})A_1(q^2) \mp \frac{2M_{D_s^+} p_{K\pi}}{M_{D_s^+} + M_{K\pi}} V(q^2)$ and $H_0(q^2) = \frac{1}{2m_{K\pi} q} [(M_{D_s^+}^2 - m_{K\pi}^2 - q^2)(M_{D_s^+} + m_{K\pi})A_1(q^2) - \frac{4M_{D_s^+}^2 p_{K\pi}^2}{M_{D_s^+} + M_{K\pi}} A_2(q^2)]$, where $p_{K\pi}$

is the momentum of the $K\pi$ system in the rest frame of the D_s^+ , and $V(q^2)$ and $A_{1/2}(q^2)$ are the vector and axial FFs, respectively. Because $A_1(q^2)$ is common to all three helicity amplitudes, it is natural to define the FF ratios $r_V = V(0)/A_1(0)$ and $r_2 = A_2(0)/A_1(0)$. The $A_{1/2}(q^2)$ and $V(q^2)$ are assumed to have simple pole forms, $A_{1/2}(q^2) = A_{1/2}(0)/(1 - q^2/M_A^2)$ and $V(q^2) = V(0)/(1 - q^2/M_V^2)$, with pole masses $M_V = M_{D^*(1-)} = 2.01 \text{ GeV}/c^2$ and $M_A = M_{D^*(1+)} = 2.42 \text{ GeV}/c^2$ [3].

We perform a five-dimensional maximum likelihood fit in the space of $M_{K^+\pi^-}^2$, q^2 , $\cos\theta_e$, $\cos\theta_K$, and χ for the $D_s^+ \rightarrow K^0 e^+ \nu_e$ events within $-0.15 < \text{MM}^2 < 0.15 \text{ GeV}^2/c^4$ in a similar manner to Refs. [24, 25]. We ignored the possible S -wave component in $K\pi$ system due to limited statistics. The projections of the fit onto $M_{K^+\pi^-}^2$, q^2 , $\cos\theta_e$, $\cos\theta_K$, and χ are shown in Figs. 3 (c-g). In this fit, the K^{*0} Breit-Wigner function follows Ref. [24], with a mass and width fixed to those reported in Ref. [3]. We obtain $r_V = 1.67 \pm 0.34(\text{stat.})$ and $r_2 = 0.77 \pm 0.28(\text{stat.})$. The fit procedure has been validated by analyzing a large inclusive MC sample, and the pull distribution of each fitted parameter was consistent with a normal distribution. The systematic uncertainties in the FF ratio measurements are estimated by comparing the nominal values with those obtained after varying one source of uncertainty, as described in Ref. [19]. The systematic uncertainties in measuring r_V (r_2) arise mainly from the uncertainties related to tracking, PID and photon detection (1.8 [2.6]%), the K^{*0} mass window (1.8 [1.3]%), the MM^2 signal region (8.7 [7.8]%), the $E_{\gamma\text{max}}$ requirement (1.2 [1.3]%), the $M_{K^0 e^+}$ requirement (0.6 [1.3]%), background estimation (1.8 [1.3]%), and the K^{*0} Breit-Wigner line shape (0.3 [1.3]%). Combining all of these in quadrature, we find the systematic uncertainties in r_V and r_2 of $D_s^+ \rightarrow K^0 e^+ \nu_e$ to be 9.3% and 8.7%, respectively.

In summary, using a data sample corresponding to an integrated luminosity of 3.19 fb^{-1} that was collected at $\sqrt{s} = 4.178 \text{ GeV}$ by the BESIII detector, we measure the absolute BFs of the CS SL decays $D_s^+ \rightarrow K^0 e^+ \nu_e$ and $D_s^+ \rightarrow K^{*0} e^+ \nu_e$ to be $\mathcal{B}(D_s^+ \rightarrow K^0 e^+ \nu_e) = (3.25 \pm 0.38(\text{stat.}) \pm 0.16(\text{syst.}) \times 10^{-3}$ and $\mathcal{B}(D_s^+ \rightarrow K^{*0} e^+ \nu_e) = (2.37 \pm 0.26(\text{stat.}) \pm 0.20(\text{syst.}) \times 10^{-3}$. These are the most precise measurements to date. Theoretical predictions of these BFs range from 2.0×10^{-3} to 3.9×10^{-3} [20, 26–29] for $D_s^+ \rightarrow K^0 e^+ \nu_e$ and 1.7×10^{-3} to 2.3×10^{-3} [20, 27–30] for $D_s^+ \rightarrow K^{*0} e^+ \nu_e$, respectively. Since the predicated BF 2.0×10^{-3} based on a double-pole model in Ref. [26] is more than 2 standard deviations away from the mean value of our measured $\mathcal{B}(D_s^+ \rightarrow K^0 e^+ \nu_e)$, thus at a confidence level of 95%, our measurement disfavors this prediction.

By analyzing the dynamics of $D_s^+ \rightarrow K^0 e^+ \nu_e$ and $D_s^+ \rightarrow K^{*0} e^+ \nu_e$ decays for the first time, we determine the FF of $D_s^+ \rightarrow K^0 e^+ \nu_e$ to be $f_+^K(0) = 0.720 \pm 0.084(\text{stat.}) \pm 0.013(\text{syst.})$ and the FF ratios of $D_s^+ \rightarrow K^0 e^+ \nu_e$ to be $r_V = 1.67 \pm 0.34(\text{stat.}) \pm 0.16(\text{syst.})$ and $r_2 = 0.77 \pm 0.28(\text{stat.}) \pm 0.07(\text{syst.})$. With the FF of $D^+ \rightarrow \pi^0 e^+ \nu_e$ measured by BESIII [21] and that of $D^+ \rightarrow \rho^0 e^+ \nu_e$ by CLEO [24],

TABLE III. The ratios of the form factors.

	Values
$f_+^{D_s^+ \rightarrow K^0}(0)/f_+^{D^+ \rightarrow \pi^0}(0)$	$1.16 \pm 0.14(\text{stat.}) \pm 0.02(\text{syst.})$
$r_V^{D_s^+ \rightarrow K^{*0}}/r_V^{D^+ \rightarrow \rho^0}$	$1.13 \pm 0.26(\text{stat.}) \pm 0.11(\text{syst.})$
$r_2^{D_s^+ \rightarrow K^{*0}}/r_2^{D^+ \rightarrow \rho^0}$	$0.93 \pm 0.36(\text{stat.}) \pm 0.10(\text{syst.})$

we calculate the ratios of the FFs of $D_s^+ \rightarrow K^0 e^+ \nu_e$ to $D^+ \rightarrow \pi^0 e^+ \nu_e$ and $D_s^+ \rightarrow K^{*0} e^+ \nu_e$ to $D^+ \rightarrow \rho^0 e^+ \nu_e$ decays, as shown in Table III, which are consistent with LQCD predictions [4]. These measurements provide a first test of the LQCD prediction that the FFs are insensitive to spectator quarks, which has important implications when considering the corresponding B and B_s decays [4, 5].

The BESIII collaboration thanks the staff of BEPCII and the IHEP computing center for their strong support. This work is supported in part by National Key Basic Research Program of China under Contract No. 2015CB856700; National Natural Science Foundation of China (NSFC) under Contracts Nos. 11335008, 11425524, 11505010, 11625523, 11635010, 11735014, 11775027; the Chinese Academy of Sciences (CAS) Large-Scale Scientific Facility Program; the CAS Center for Excellence in Particle Physics (CCEPP); Joint Large-Scale Scientific Facility Funds of the NSFC and CAS under Contracts Nos. U1532257, U1532258, U1732263; CAS Key Research Program of Frontier Sciences under Contracts Nos. QYZDJ-SSW-SLH003, QYZDJ-SSW-SLH040; 100 Talents Program of CAS; INPAC and Shanghai Key Laboratory for Particle Physics and Cosmology; German Research Foundation DFG under Contracts Nos. Collaborative Research Center CRC 1044, FOR 2359; Istituto Nazionale di Fisica Nucleare, Italy; Koninklijke Nederlandse Akademie van Wetenschappen (KNAW) under Contract No. 530-4CDP03; Ministry of Development of Turkey under Contract No. DPT2006K-120470; National Science and Technology fund; The Swedish Research Council; U. S. Department of Energy under Contracts Nos. DE-FG02-05ER41374, DE-SC-0010118, DE-SC-0010504, DE-SC-0012069; University of Groningen (RuG) and the Helmholtzzentrum fuer Schwerionenforschung GmbH (GSI), Darmstadt; This paper is also supported by Beijing municipal government under Contract Nos. KM201610017009, 2015000020124G064, CIT&TCD201704047.

- [2] J. Yelton, *et al.* [CLEO Collaboration], Phys. Rev. D **80**, 052007 (2009).
- [3] C. Patrignani *et al.* [Particle Data Group], Chin. Phys. C **40**, 100001 (2016) and 2017 update.
- [4] J. Koponen, C. T. H. Davies and G. Donald [HPQCD Collaboration], arXiv:1208.6242 (2012); J. Koponen, C. T. H. Davies, G. C. Donald, E. Follana, G. P. Lepage, H. Na and J. Shigemitsu [HPQCD Collaboration], arXiv:1305.1462 (2013).
- [5] J. A. Bailey, A. Bazavov, C. Bernard *et al.*, Phys. Rev. D **85**, 114502 (2012).
- [6] M. Ablikim *et al.* [BESIII Collaboration], Nucl. Instrum. Meth. A **614**, 345 (2010).
- [7] S. Agostinelli *et al.* [GEANT4 Collaboration], Nucl. Instrum. Meth. A **506**, 250 (2003).
- [8] R. G. Ping, Chin. Phys. C **38**, 083001 (2014).
- [9] E. A. Kurav and V. S. Fadin, Sov. J. Nucl. Phys. **41**, 466 (1985).
- [10] D. J. Lange, Nucl. Instrum. Meth. A **462**, 152 (2001); R. G. Ping, Chin. Phys. C **32**, 599 (2008).
- [11] E. Richter-Was, Phys. Lett. B **303**, 163 (1993).
- [12] K. A. Olive *et al.* [Particle Data Group], Chin. Phys. C **38**, 090001 (2014) and 2015 update.
- [13] J. C. Chen, G. S. Huang, X. R. Qi, D. H. Zhang and Y. S. Zhu, Phys. Rev. D **62**, 034003 (2000).
- [14] D. Cronin-Hennessy *et al.* [CLEO Collaboration], Phys. Rev. D **80**, 072001 (2009).
- [15] M. Ablikim *et al.* [BESIII Collaboration], Phys. Rev. Lett. **118**, 112001 (2017); Phys. Lett. B **772**, 388 (2017).
- [16] M. Ablikim *et al.* [BESIII Collaboration], Phys. Rev. D **92**, 112008 (2015); Phys. Rev. D **92**, 071101(R) (2015).
- [17] M. Ablikim *et al.* [BESIII Collaboration], Phys. Rev. Lett. **115**, 221805 (2015).
- [18] P. del Amo Sanchez *et al.* [BaBar Collaboration], Phys. Rev. D **83**, 072001 (2011).
- [19] M. Ablikim *et al.* [BESIII Collaboration], Phys. Rev. D **94**, 032001 (2016).
- [20] W. Wang and Y. L. Shen, Phys. Rev. D **78**, 054002 (2008).
- [21] M. Ablikim *et al.* [BESIII Collaboration], Phys. Rev. D **96**, 012002 (2017).
- [22] D. Becirevic and A. B. Kaidalov, Phys. Lett. B **478**, 417 (2000).
- [23] T. Becher and R. J. Hill, Phys. Lett. B **633**, 61 (2006).
- [24] S. Dobbs *et al.* [CLEO Collaboration], Phys. Rev. Lett. **110**, 131802 (2013).
- [25] M. Ablikim *et al.* [BESIII Collaboration], Phys. Rev. D **92**, 071101(R) (2015).
- [26] S. Fajfer and J. Kamenik, Phys. Rev. D **71**, 014020 (2005).
- [27] D. Melikhov and B. Stech, Phys. Rev. D **62**, 014006 (2000).
- [28] Y. L. Wu, M. Zhong and Y. B. Zuo, Int. J. Mod. Phys. A **21**, 6125 (2006).
- [29] H. Y. Cheng and X. W. Kang, Eur. Phys. J. C **77**, 587 (2017).
- [30] S. Fajfer and J. Kamenik, Phys. Rev. D **72**, 034029 (2005).

[1] M. B. Voloshin, Phys. Lett. B **515**, 74 (2001); D. Scora and N. Isgur, Phys. Rev. D **52**, 2783 (1995).